Materials Advances

ROYAL SOCIETY OF CHEMISTRY

PAPER

View Article Online
View Journal | View Issue



Cite this: *Mater. Adv.*, 2022, 3, 3500

# Untangling the controversy on $Ce^{3+}$ luminescence in $LaAlO_3$ crystals†

Jan Pejchal, *[a] Vladimir Babin, [a] Maksym Buryi, [a] Valentyn Laguta, [a] František Hájek, [ab] Juraj Páterek, [ab] Lenka Procházková-Prouzová, [ab] Lubomír Havlák, [a] Vladimíra Czerneková, [a] Vojtěch Vaněček, [ab] Václav Doležal, [c] Jan Havlíček, [c] Kateřina Rubešová, [c] Petra Zemenová, [a] Alexandra Falvey, [d] Robert Král, [a] Vladimir Pankratov [e] and Kirill Chernenko [f]

Aluminum perovskites represent an important group of promising scintillation materials with excellent proportionality and energy resolution, but due to difficulties in crystal growth not much attention has been paid to them. We studied a Ce-doped $LaAlO_3$ lanthanum–aluminum perovskite (LaAP) because of its easy crystal growth facilitated by the large $La^{3+}$ cations in the matrix. Moreover, recent observations of intense blue luminescence by some researchers show that the potential of this material could not be ruled out. On the other hand, some reports claim that $Ce^{3+}$ luminescence is completely absent in the LaAP matrix. Therefore, we have decided to study this material in much greater detail using an extended set of correlated experiments to explain the observed discrepancies and underlying phenomena. Crystal growth by the micro-pulling-down method is reported together with the luminescence and scintillation properties. We demonstrate the influence of inclusions of other aluminate phases created during the crystal growth on the luminescence processes. The existence of the phases was simultaneously confirmed by observations using a scanning electron microscope, cathodoluminescence, energy-dispersive X-ray analysis and electron paramagnetic resonance (EPR), which were correlated with photoluminescence and scintillation studies. The EPR evidenced the incorporation of Ce ions in different environments comprising the LaAP matrix and inclusions. Based on these results, the luminescence mechanism is proposed and discussed and the low scintillation efficiency of the Ce-doped LaAP is explained together with the discrepancies in the literature.

Received 17th November 2021,
Accepted 1st March 2022

DOI: 10.1039/d1ma01083b

rsc.li/materials-advances



## 1. Introduction

Scintillation materials are applied in the detection of ionizing radiation and related fields of science and technology, such as medical imaging, high-energy physics, industrial defectoscopy, geological survey and oil well logging, astronomy, homeland security and others.[1–3] The recent development of medical imaging applications employing scintillators has been driven by an increased need for non- or minimally invasive *in vivo* examination.[4] Last but not least we can mention environmental monitoring, which has been intensified also with the development of unmanned vehicles utilized for example in the area of the Fukushima[5] or Chernobyl nuclear power plants.[6]

Scintillation detectors for all these applications mostly employ inorganic materials based on single crystals of garnets,[7,8] heavy silicates,[9–12] halides[13–17] or other multicomponent compounds.[1,2,9,18,19]

Aluminum perovskites constitute another important group of scintillation materials.[20] Due to difficulties in crystal growth they have not received enough attention so far, but many of them show very competitive practical parameters. The reported decay time of the Ce-doped $YAlO_3$ (yttrium aluminum perovskite, YAP) luminescence, as short as 18 ns, is among the fastest in Ce-doped oxides.[20,21] Furthermore, very small nonproportionality in the YAP:Ce scintillation response results in its excellent energy resolution.[2] This parameter is crucial for medical imaging or environmental monitoring, where high-energy photons of close energies need to be resolved.[4] Its rather

[a] *Institute of Physics, Czech Academy of Sciences, Cukrovarnická 10, Prague, Czech Republic. E-mail: pejchal@fzu.cz*
[b] *Faculty of Nuclear Sciences and Physical Engineering, Czech Technical University in Prague, Břehová 7, Prague, Czech Republic*
[c] *Department of Inorganic Chemistry, University of Chemistry and Technology, Technická 5, 166 28, Prague 6, Czech Republic*
[d] *Masaryk Secondary School of Chemistry, Křemencova 179/12, 116 28, Prague, Czech Republic*
[e] *Institute of Solid State Physics, University of Latvia, 8 Kengaraga, LV-1063 Riga, Latvia*
[f] *MAX IV Laboratory, Lund University, P.O. Box 118, SE-22100 Lund, Sweden*

† Electronic supplementary information (ESI) available. See DOI: 10.1039/d1ma01083b

low density and an effective atomic number of 5.37 g $cm^{-3}$ and 33.5, respectively, and the resulting low stopping power for high-energy photons are, however, the major disadvantages of this material. Its heavier structural analog, $LuAlO_3$ (LuAP) with a high density of 8.35 g $cm^{-3}$ and an effective atomic number as high as 64.9, has attracted attention from the scintillation material community since 1990s.[22–25] However, due to the very low stability of the perovskite phase and difficulties in crystal growth, its commercialization was not successful even in the case of a more stable Y-admixed LuAP (LuYAP) variant.[26] Similar to the garnet counterparts,[7–9] the anti-site defects (rare-earth ions substituting $Al^{3+}$ in the $AlO_6$ octahedra) and related deterioration of scintillation characteristics can also be observed in perovskites.[27] This is also why the performance of perovskite-based scintillation materials is well below the estimated fundamental limits[28] and there is still considerable room for their optimization or even the search for new perovskite-based systems.

Another perovskite material is the compositional analogue $LaAlO_3$ (LaAP), whose crystal growth is much easier due to its favorable structural features. It has almost an ideal value of the so called Goldschmidt tolerance factor,[29,30] which indicates the stability of the perovskite phase. The phase stability increases as the tolerance factor approaches unity. On the other hand, $LaAlO_3$ has a phase transition from the $Pm\bar{3}m$ cubic to rhombohedral $R\bar{3}c$ structure below 430 °C.[31] The transition occurs gradually and is of an order higher than first order.[31] This was confirmed also by spectroscopic measurements for the $Eu^{3+}$ lines in the Eu-doped LaAP, where the symmetry of the $Eu^{3+}$ site and the resulting spectra gradually change near the phase transition temperature.[32] The phase transition is non-destructive and therefore crystal growth from the melt is possible.

The luminescence and scintillation properties of the LaAP:Ce single crystals together with Tb and Eu-doped ones and the influence of the growth atmosphere were studied recently by some of us.[33] It was found that the band-to-band transition in the undoped sample was at 225 nm, which was in accordance with the earlier reports.[28,34] The samples with a lower Ce concentration (up to 1 at%) showed $Ce^{3+}$ 4f–5d transitions around 310–320 nm and 245 nm, which would also correspond to the previously reported results.[35–37] For heavily Ce-doped samples grown under a $N_2$ atmosphere a very strong absorption band emerged below 550 nm and practically disappeared for the counterparts grown under an Ar + 5%$H_2$ atmosphere. This phenomenon was ascribed to an insufficient reduction of $Ce^{4+}$ in the crystals grown in the $N_2$ atmosphere, since Ce was introduced in the form of $CeO_2$.[33] The radioluminescence efficiency of the Ce-doped samples was found to be very low regardless of the growth atmosphere and Ce concentration. On the other hand, it was very high for the $Tb^{3+}$ and $Eu^{3+}$-doped samples, especially in the latter case, which most probably indicated that luminescence centers acting as electron acceptors are more efficient in this material. This fact was used to partially explain the low efficiency of the Ce-doped samples, since $Ce^{3+}$ ions are hole acceptors.[33] The photoluminescence emission spectra of the selected Ce-doped samples were significantly different from those of the radioluminescence ones and showed an unusually high Stokes shift, which has made the understanding of the luminescence mechanism difficult so far. A significant role of the perturbed $Ce^{3+}$ centers was suggested[33] in the luminescence mechanism of this material, assuming similar phenomena considered in the $CeF_3$ single crystals.[38]

Weak luminescence was observed under UV excitation for cerium–aluminum perovskite crystals with a tetragonal structure, where La is entirely replaced by Ce (CeAP). No scintillation was found under X-ray excitation.[39]

The growth of the undoped and Ce-doped LaAP (LaAP:Ce) by the Czochralski method was described by Zeng *et al.*,[35] where a reasonably high Ce segregation coefficient of 0.28 was found. Under 317 nm excitation, the Ce-doped crystal showed luminescence at 410 nm, which was ascribed to the $Ce^{3+}$ 5d–4f transition. In contrast, a complete absence of $Ce^{3+}$ luminescence was reported in the LaAP host much earlier.[36] This was later explained by van der Kolk *et al.* who used photocurrent spectroscopy, which revealed strong ionization of the $Ce^{3+}$ 5d excited states supposedly entirely buried in the conduction band.[37] It is necessary to emphasize that no details on the growth of the crystal were given at all in the study where no luminescence was observed.[37] On the other hand, in the study reported by Zeng *et al.*,[35] where blue luminescence was observed in LaAP:Ce, the crystal growth is reported in great detail, while the luminescence properties are not deeply analyzed.

Apparently, controversy about Ce emission in LaAP still remains. Due to the above mentioned significant application potential of aluminum perovskites it is highly desirable to reveal the cause of such discrepancies, verify and evaluate the luminescence phenomena in the LaAP:Ce single crystal and finally confirm or exclude its suitability for the scintillation applications.

It appears critical to understand the morphology of this material on a microscopic scale and its relationship with the luminescence properties to clarify the observed phenomena, which has not been done so far.

In this article we demonstrate the complex nature of the luminescence and energy storage processes in LaAP:Ce involving Al-rich phases created in the material. We use a broad portfolio of experimental techniques including electron paramagnetic resonance (EPR), which helped to reveal the sites where the $Ce^{3+}$ ion is stabilized. To the best of our knowledge, the $Ce^{3+}$ EPR spectrum has never been measured in $LaAlO_3$ crystals or even in the $LaAlO_3$–$CeAlO_3$ solid solutions although in the other aluminum perovskites (*e.g.* $YAlO_3$, $LuAlO_3$) the $Ce^{3+}$ EPR spectrum is very well visible.[40,41] The correlated experiments allowed us to finally explain the discrepancies in various studies involving the observation[35] or absence[36,37] of luminescence in LaAP:Ce crystals and to infer their scintillation application potential.

## 2. Experimental details

### 2.1. Crystal growth

The crystals were grown by the micro-pulling-down method[42,43] as was described already elsewhere;[33] however, we would like to

mention the most important crystal growth parameters again. The growth was performed in an iridium crucible with a die of 5 mm in diameter with 5 capillaries. An iridium wire was used as a seed and the pulling speed was 0.15 mm $min^{-1}$. The starting materials were prepared by mixing 4N purity $La_2O_3$, $Al_2O_3$ and $CeO_2$ from Alfa Aesar. The nominal Ce concentrations ranged from 0 to 100 at% with respect to La. Some crystals were grown under an $N_2$ atmosphere and other ones under an Ar + 5%$H_2$ atmosphere. An undoped sample was grown as well under an $N_2$ atmosphere.

The crystals grown were of cylindrical shape with 5 mm diameter and around 17 mm in length.[33] A thin plate was cut from each crystal and was polished to a thickness of 1 mm for further characterization.

Since we suspected possible influence of $La_2O_3$ hygroscopicity on the weighing errors resulting in sample non-stoichiometry and Al-rich phases creation, a new analogous series of crystals were prepared from the pre-heated $La_2O_3$ starting powder. The pre-heating procedure was optimized according to differential scanning calorimetry, thermogravimetric analysis and mass spectrometry (DSC-TGA/MS) (Fig. S1 in the ESI†). The samples studied in this work comprise some of the samples studied earlier[33] and the new samples were grown from the pre-heated $La_2O_3$ with a balanced stoichiometry. All of them are summarized in Table S1 in the ESI† together with the growth atmospheres. The samples will be further denoted with an acronym composed of a number indicating the Ce concentration, N2 or H2 sign for $N_2$ or Ar + $H_2$ growth atmosphere, and the BS abbreviation for the samples with the balanced stoichiometry. The acronyms without the abbreviation refer to the samples with unbalanced stoichiometry, see Table S1 in the ESI.†

As mentioned above, we have also prepared samples with higher Ce concentrations including 50% and 100% Ce. However, these samples were used only for EPR measurements, while their luminescence characteristics have been found to be extremely complicated and will not be included here.

### 2.2. Powder preparation

To better understand the phenomena related to the other aluminum-rich phases created during crystal growth, the powder samples of the considered $LaAl_{11}O_{18}$ lanthanum hexaaluminate (LHA) phases were prepared *via* a solid state reaction and $La_{0.86}Al_{11.9}O_{19.14}$ magnetoplumbites (MP) *via* sol–gel co-precipitation in the form of pellets.

For comparison, LaAP:Ce powder samples with a composition of $Ce_xLa_{1-x}AlO_3$ ($x$ = 0.001 and 0.01) were also prepared.

For details on the powder sample preparation and analyses refer to the ESI.†

### 2.3. Absorption and luminescence spectroscopy

The luminescence measurements were performed using a modified spectrofluorometer (custom made 5000M model, Horiba Jobin Yvon) equipped with a TBX-04 photon counting detector (IBH Scotland). A deuterium steady-state lamp (Heraeus) was used for the excitation and emission spectra measurements. An X-ray tube operating at a voltage of 40 kV and 15 mA current with a tungsten anode (Seifert GmbH.) was used as the excitation source for radioluminescence (RL) measurements. Since the scintillation material is intended for measurements and monitoring of ionizing radiation, radioluminescence is an excellent tool to evaluate its overall scintillation efficiency, especially when a standard material is used for relative comparison. In our case the standard material was $Bi_4Ge_3O_{12}$ (BGO). All the spectra were corrected for experimental distortions caused by the setup. The hydrogen nanosecond flashlamp or pulsed nanoLED source (IBH Scotland) was used for luminescence decay measurements using the methods of time correlated single photon counting. Exponential fits of the decays were obtained by performing the convolution of the considered function with the instrumental response and a least-square sum fitting procedure (SpectraSolve software package from Ames Photonics).

### 2.4. Electron microscopy, X-ray microanalysis and cathodoluminescence

The cathodoluminescence (CL) and energy-dispersive X-ray spectroscopy (EDX) measurements were performed using a FEI XL30 ESEM scanning electron microscope (SEM). The EDX mapping and the CL measurements were carried out with a 30 kV acceleration voltage. The CL home-build setup consists of a single-grating monochromator with a spectral resolution of 10 nm and the Hamamatsu H7711-13 photomultiplier tube for CL images and the Avaspec ULS2048LTEC spectrometer for recording spectra. For spectra acquisition, a sample area of 23 × 15 μm was scanned. The spectra were corrected for the spectral sensitivity of the setup.

### 2.5. Electron paramagnetic resonance

The EPR measurements were performed in the X-band (9.4 GHz) with a commercial Bruker EMX spectrometer at temperatures from 6–296 K. The X-ray irradiation of the samples was performed at the liquid nitrogen temperature using an ISO-DEBYEFLEX 3003 highly stabilized X-ray equipment for structure analysis (tungsten X-ray tube, 50 kV, 30 mA). The spectral intensity in all cases was normalized to 1 g of the sample weight.

To study the thermal stability of the charge trapping centers the pulse annealing method was applied. The sample was X-ray-irradiated at the liquid nitrogen temperature. Then, the sample temperature was lowered until the EPR signals appearing after the X-ray irradiation reached the best signal-to-noise ratio (before the saturation). This is the fixed temperature. After this, the sample was quickly heated up to a certain annealing temperature, held there for a time period enough for good thermalization (4 minutes is usually a good choice) and, subsequently, the sample was cooled down fast to the fixed temperature. This procedure is repeated cycle by cycle by increasing the annealing temperature every time until the thermally depopulated centers responsible for the signal studied are depleted.

# 3. Results and discussion

## 3.1. Crystal growth and powder preparation

The undoped and Ce-doped LaAP single crystals were successfully grown by the micro-pulling-down method under an $N_2$ or Ar + 5%$H_2$ atmosphere. The crystals were of a single phase of the rhombohedral low temperature LaAP modification showing some mosaicity due to sub-grains as was already reported.[33]

The lanthanum hexaaluminate ($LaAl_{11}O_{18}$, LHA) powder samples were successfully prepared *via* the solid state reaction avoiding the formation of any LaAP phase. The XRD analysis (ESI,† paragraphs 2.1., 2.2) has shown that the samples contained mostly some other kind of MP phase described by chemical formula $La_{0.827}Al_{11.9}O_{19.09}$ corresponding to the JCPDS 01-077-0311 database pattern. Some samples contained a minor impurity phase of the metastable LHA superstructure $La_2Al_{22}O_{36}$ (JCPDS 00-028-0502).

The powder samples prepared by the Pechini sol gel process with $La_{0.86}Al_{11.9}O_{19.14}$ magnetoplumbite (MP) stoichiometry contained the $Al_2O_3$ parasitic phase, whose amount increased with increasing Ce concentration from 4 to 13% (corresponding to the Ce concentration from 0% Ce to 100%).

The co-precipitated $Ce_xLa_{1-x}AlO_3$ ($x$ = 0.001 and 0.01) samples were both single-phase with a rhombohedral crystal structure. See the ESI† (paragraphs 2.3. and 2.4.) for details.

## 3.2. Optical, luminescence and scintillation properties

The absorption spectra of the samples with low Ce concentration and balanced stoichiometry grown under the Ar + 5%$H_2$ atmosphere are shown in Fig. 1. The $Ce^{3+}$ 4f–5d absorption bands at 245 and 317 nm can be observed already for the lowest Ce concentration of 0.001% and can be best resolved for 0.01% Ce, while the saturation of the signal already occurs at 0.1% Ce. These bands were observed before[35–37] and the 317 nm one can be ascribed to the $E_g$ doublet formed by $z^2$ and $x^2 - y^2$ 5d orbitals, while the high-energy band at 245 nm is a $T_{2g}$ triplet composed of $xy$, $xz$ and $yz$ 5d orbitals, as was shown by theoretical calculations.[44,45] The samples with a low Ce concentration were chosen to study these transitions more precisely. For the absorption spectra of some of the other samples see the previous report.[33]

The radioluminescence (RL) spectra of the samples with unbalanced stoichiometry were already shown and discussed elsewhere.[33] Regardless of the growth atmosphere, a very weak broad-band emission was observed around 400 nm and was tentatively ascribed to defects, as it was practically independent of the Ce concentration. Emission found at 700 nm was ascribed to $Cr^{3+}$ impurity.

Fig. 2 compares the RL spectra of 20-H2-BS and 30-H2-BS samples with those of the BGO standard material. The amplitude of the former is again very low (it is in the original scale, while BGO is divided by 100) and the peak is shifted towards shorter wavelengths around 360 nm, while the amplitude of the latter reaches almost as high as half of that of BGO, which is a very unusual observation indeed. Note that this spectrum for the 30-H2-BS sample is divided by 100 as well and is therefore directly comparable to that of BGO in Fig. 2. It is necessary to mention that this particular sample was prepared from the seed part (*i.e.* the very beginning) of the 30-H2-BS crystal, while the samples cut from the other parts showed RL spectra very similar to those of the 20-H2-BS sample in Fig. 2. To further understand the above observations, thorough photoluminescence (PL) measurements need to be performed. Even though the luminescence intensity observed for all the samples is quite low and most of the respective spectra are noisy, relevant and reliable data could be often obtained.

**3.2.1. Selected photoluminescence results of the samples with unbalanced stoichiometry grown under the Ar + $H_2$ atmosphere.** Since the absorption characteristics of the samples

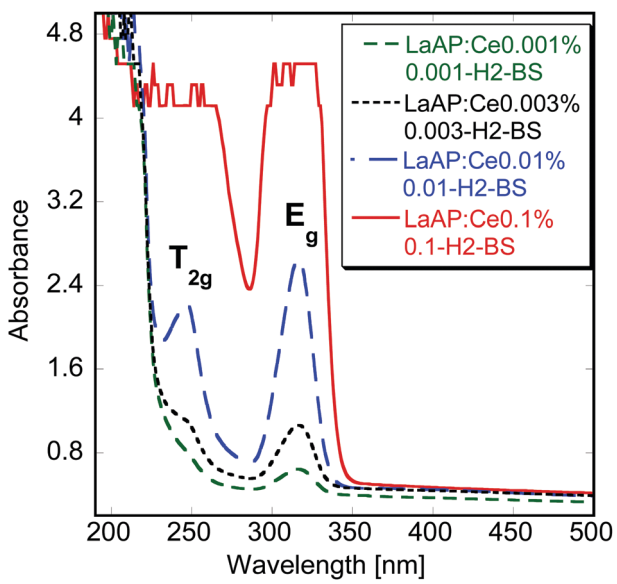


Fig. 1 Absorption spectra of the samples with balanced stoichiometry and low Ce concentration.

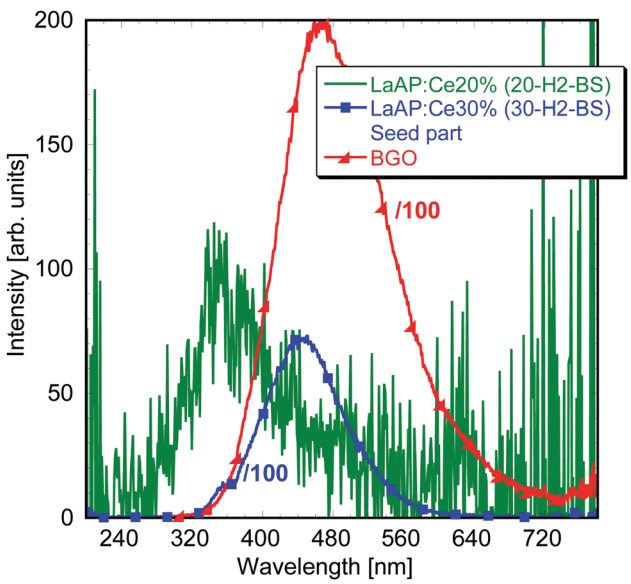


Fig. 2 Radioluminescence spectra of the LaAP:Ce samples with balanced stoichiometry with higher Ce concentration.

grown under the Ar + $H_2$ atmosphere point to the better incorporation of Ce into the LaAP matrix,[33] more reliable photoluminescence characteristics are expected.

The photoluminescence emission spectrum of the LaAP:Ce1% 1-H2 sample under 250 nm excitation (close to the $Ce^{3+}$ absorption from the 4f state to the $T_{2g}$ triplet, similar as in Fig. 1) is shown in Fig. 3a. There is quite a prominent band at 370 nm and a shoulder at 440 nm. The same luminescence processes can be found in the $N_2$-grown counterparts, but here they can be better resolved. An interesting finding is the absence of the $Cr^{3+}$ impurity emission around 740 nm observed in the 0-N2 sample under the same excitation wavelength,[33] while the longer wavelength 580 and 660 nm peaks emerge in the 1-H2 sample. It might be that there is an interaction between the Ce dopant and the Cr impurity, which can result in the Ce-terminated $Cr^{3+}$ emission observed earlier in the Ce-doped YAP[20] and in the disappearance of the $Cr^{3+}$ emission that originates purely in its 3d electron shell. Regarding the peak wavelengths, an attempt to ascribe them to these transitions was made according to the data reported by Luo and Dorenbos,[46] where the so-called vacuum-referred binding energy (VRBE) scheme[47] of the trivalent rare-earth ground state positions in LaAP together with the $Cr^{3+}$ states is displayed, see Fig. 11 in the paper by Luo and Dorenbos.[46] Considering the

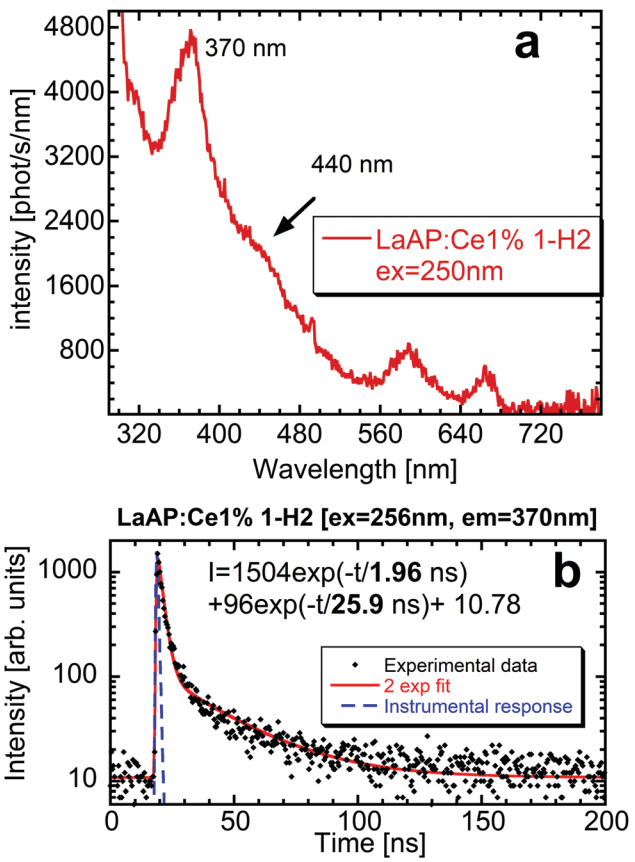


Fig. 3 Emission spectrum of the LaAP:Ce1% sample grown under the Ar + $H_2$ atmosphere (1-H2) under 250 nm excitation (a) and the decay time of the 370 nm emission under 256 nm excitation for the same sample (b).

$Ce^{3+}$ 4f ground state at −5.2 eV, then the transition from the $Cr^{3+}$ $^4T_1(^4F)$ state located at −3.35 eV and terminated at the $Ce^{3+}$ ground state would result in a peak around 551 nm, which is not very far from the observed value of 580 nm. The difference might be caused by some unknown perturbing phenomena or partially also by the simplifications considered in the VRBE model.[47] Or the peak might be of some other unknown origin. These considerations still cannot explain the origin of the 660 nm peak, which is probably more complicated. The emission intensity at 370 nm was high enough to perform decay kinetics measurements (Fig. 3b). The photoluminescence decay curve of the 370 nm emission peak under 256 nm excitation consists of one very fast component with a decay time of around 2 ns and another one with a decay time of about 26 ns. The very fast luminescence process can originate from some defects, most probably related to some $F^+$-centers, whose creation can be facilitated by the reducing growth atmosphere. Considering the 25 ns component and the emission position at 370 nm, these values are not very far from those observed for the $Ce^{3+}$ 5d–4f emission in YAP.[20] To verify the 370 nm emission origin, it is necessary to find what could be the emission wavelength of the regular $Ce^{3+}$, if it showed luminescence in the LaAP matrix.

The predictive behavior of the $Ce^{3+}$ 5d–4f emission in various multicomponent oxide matrices was systematically treated by Dorenbos[48] and it follows from these studies that the $Ce^{3+}$ emission would appear at much shorter wavelengths in LaAP around 340 nm, see the considerations in the ESI† in paragraph 3. Therefore, the emission at 370 nm in Fig. 3a is not related to the regular $Ce^{3+}$ in the LaAP matrix.

The already reported[33] temperature dependence of the photoluminescence of the LaAP:Ce20% 20-H2 counterpart did not bring a deeper insight into the luminescence phenomena in the LaAP:Ce crystals. The broad peaks emerging at lower temperatures were tentatively ascribed to some perturbed $Ce^{3+}$ centers present in the LaAP matrix.[33] However, further research on the samples with balanced stoichiometry has shown that the underlying phenomena are substantially different.

**3.2.2. Luminescence of the samples with the balanced stoichiometry grown under the Ar + $H_2$ atmosphere.** To study the luminescence processes in detail, we have focused on the 30-H2-BS sample, which attracted our attention due to a quite intense RL spectrum of its seed part, shown in Fig. 2. The SEM image of a polished part cut from the crystal next to the seed part is shown in Fig. 4. Apparently, the crystal contains some inclusions of tens of micrometers in size. The EDX analysis using the SEM electron beam revealed that these inclusions are strongly aluminum-rich (see the analysis table in the Fig. 4), but their exact composition could not be determined and did not correspond to any known Al-rich compound. They contain a considerable amount of Ce. The SEM electron beam was also used to study the cathodoluminescence properties. The LaAP crystal matrix itself showed no or negligible emission. On the other hand, the inclusions displayed in Fig. 4 showed a spectrum with well observable emission peaks situated around 370 and 450 nm, see Fig. 5. The spectrum resembles the

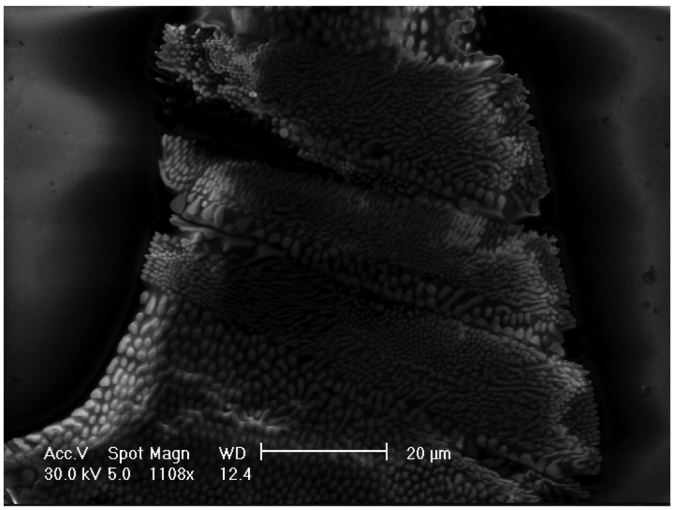


| Elem. | At % |
|---|---|
| O | 57.22 |
| Al | 36.88 |
| La | 3.92 |
| Ce | 1.98 |
| Total | 100.00 |

Fig. 4 The SEM image of the 30-H2-BS sample together with the analysis using an electron beam.

emission features observed for example in the PL spectrum of the 1-H2 sample in Fig. 3a and especially the RL spectrum for the seed part of the 30-H2-BS sample in Fig. 2. This means that the seed part of 30-H2-BS probably contains a considerable amount of such inclusions responsible for the RL characteristics. The 1-H2 sample contains the inclusions as well, which is expected due to its unbalanced stoichiometry, but their concentration in this particular sample is not high enough to influence the RL spectrum already reported.[33] On the other hand, the luminescence of the inclusions can be probably still observed in its PL spectrum shown in Fig. 3a, which consists of the 370 nm peak and a shoulder around 440 nm. These findings are also in agreement with the discussion in paragraph 3 of the ESI† which concludes that the 370 nm emission cannot be related to a regular $Ce^{3+}$ center in the LaAP matrix. It is reasonable to suppose that the emission is related to $Ce^{3+}$ incorporated to the inclusions.

The blue emission around 450 nm observed in the radioluminescence of the 30-H2-BS sample is not that far from the emission already observed by Zeng *et al.*[35] To further understand its origin, it is necessary to look at the photoluminescence of the 30-H2-BS sample in detail.

The photoluminescence spectra of the 30-H2-BS sample are compared in Fig. 6. The emission spectrum under 245 nm excitation (corresponding to the $4f–5d_2$ absorption band of $Ce^{3+}$, see Fig. 6a) is dominated by a broad emission band at 450 nm with a shoulder at 370 nm, which are features very similar to those observed in the RL spectrum of the seed part in Fig. 2 or in the cathodoluminescence spectrum of the inclusion

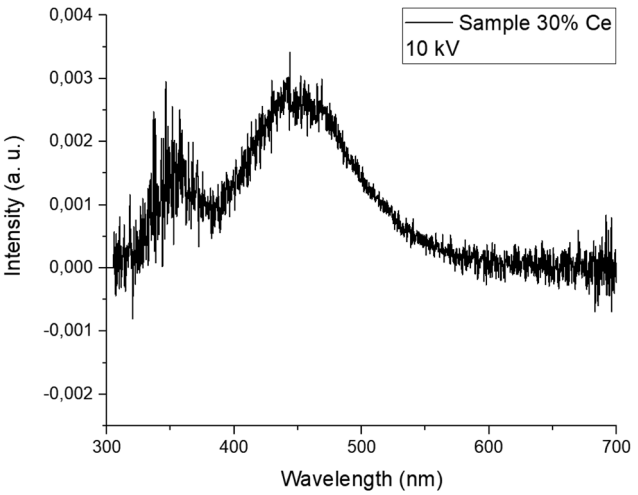


Fig. 5 Cathodoluminescence of the Al-rich micro-inclusion in the 30-H2-BS sample under SEM electron beam excitation.

in Fig. 5. This again supports the idea that the luminescence characteristics of the 30-H2-BS sample are determined by the presence of the Al-rich inclusions. The increase of the intensity at the short wavelength near 300 nm cannot be explained until now, but maybe it is a combination of the scattered light and the background value promoted by the correction for the experimental distortions. The excitation spectrum of the 370 nm emission was quite noisy and not well-resolved peaks at 310 nm and another around 240–260 nm were found

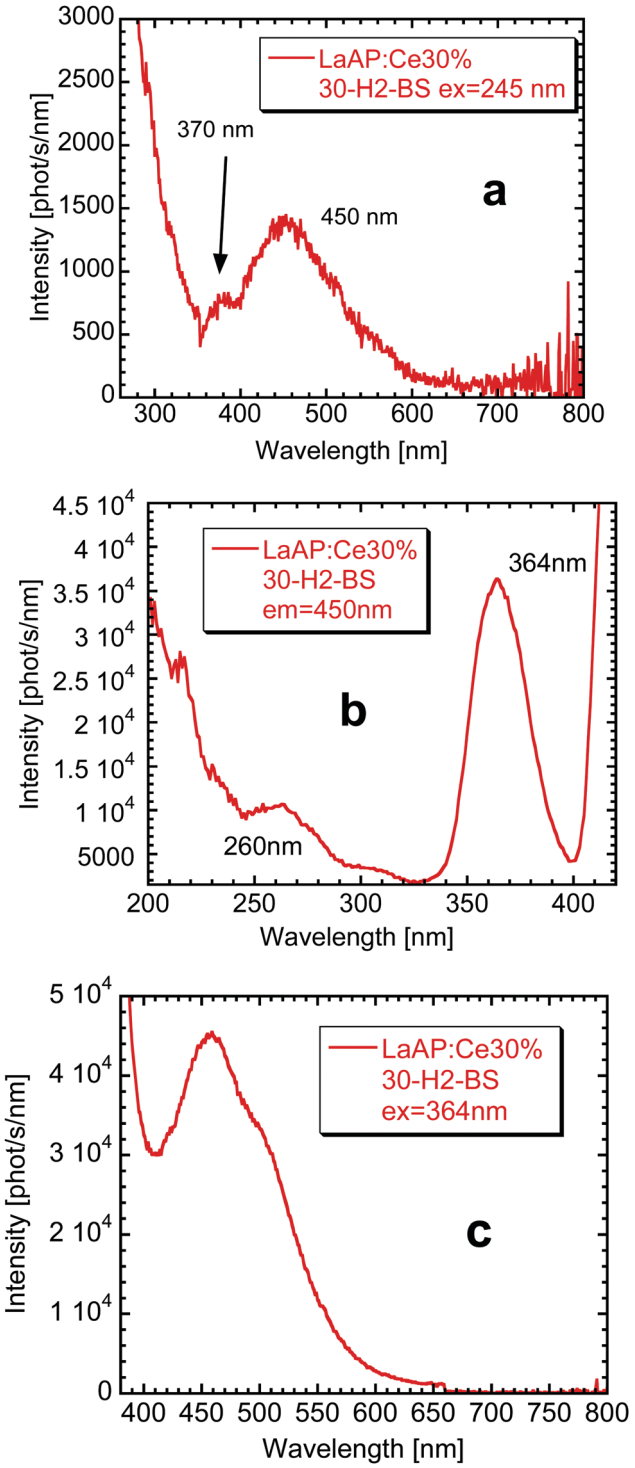


Fig. 6 Photoluminescence of the 30-H2-BS sample (LaAP:Ce 30%). Emission spectrum under 245 nm excitation (a), excitation spectrum for the 450 nm emission (b) and emission spectrum for the 364 nm excitation (c).

(not shown here). These values are similar to the $Ce^{3+}$ absorption bands shown above in Fig. 1 but they are not exactly the same. This would also mean that these characteristics belong to the $Ce^{3+}$ luminescence center incorporated to a different environment of the Al-rich inclusion.

The excitation spectrum of the 450 nm emission wavelength is displayed in Fig. 6b. Besides the small excitation band around 260 nm, there is an intense one at 364 nm. The excitation at the latter wavelength indeed leads to a relatively intense and maybe complex broad band centered around 450 nm (Fig. 6c). The 364 nm excitation peak certainly overlaps with the 370 nm emission and therefore an energy transfer between the center emitting at 370 nm towards the center emitting around 440–450 nm is expected to take place. Similar phenomenon probably takes place also for the 1-H2 sample, only the intensities are redistributed in a different manner, see Fig. 3a.

There is a question: what Al-rich phases are the inclusions composed of. The first option might be that $LaAl_{11}O_{18}$ is found in most of the phase diagrams of the $La_2O_3$–$Al_2O_3$ system.[49] However, $LaAl_{11}O_{18}$ has been studied as a phosphor host for various rare earth ions,[50,51] but no $Ce^{3+}$ or host emissions were reported to the best of our knowledge. It is also interesting to mention that atomistic simulations have shown that $LaAl_{11}O_{18}$ tends to be nonstoichiometric forming the $La_{0.83}Al_{11.83}O_{19}$ compound having a magnetoplumbite structure, which may coexist also with another structural analogue $LaAl_{11.67}O_{19}$.[52] The luminescence properties of Ce-doped magnetoplumbite of a different stoichiometry described by the formula $La_{0.86}Al_{11.9}O_{19.14}$ have been reported by Stevels.[53] When the Ce concentration at the La site varied from 2 mol% to 100 mol%, the luminescence properties drastically changed. For the lowest Ce concentration, the material showed a short-wavelength emission ascribed to a regular $Ce^{3+}$ occupying the La site and peaking around 330–350 nm. Its lowest excitation band is reported to be around 305 nm,[53] which is not very far from the 310 nm excitation band for the 370 nm emission in the 30-H2-BS sample mentioned above. With the increase of the Ce concentration, this band shifts towards slightly longer wavelengths and its intensity decreases at the expense of the broad band peaking in the blue spectral region around 430 nm, which was ascribed to an emission of the Ce–O associates.[53] Its lowest excitation band is reported to occur around 370 nm,[53] which is again close to the value in the excitation spectrum for the blue emission in Fig. 6b of the 30-H2-BS sample. The formula $La_{0.86}Al_{11.9}O_{19.14}$ suggests that 14% of the La sites are replaced by oxygen, which forms the Ce–O associates with the nearby $Ce^{3+}$ cation. The exchange of the intensities was explained by the energy transfer from the regular $Ce^{3+}$ towards the blue emission center related to the Ce–O associates. The energy transfer between the regular $Ce^{3+}$ and the Ce–O associates in the Al-rich La magnetoplumbites was described using the Förster model,[53] where the regular $Ce^{3+}$ acts as a sensitizer and the Ce–O associate as an activator, while the transfer between the sensitizers is absent. The reported luminescence bands[53] are similar to those observed for the samples above in Fig. 2, 3a, 5, or 6a, though their wavelengths are not exactly the same. But the change of their mutual intensities for different Ce concentrations is apparent for example from the PL emission spectra for the 1-H2 sample (Fig. 3a) and 30-H2-BS sample (Fig. 6a). As was already stated, the emission at 370 nm in the

30-H2-BS sample overlaps with the excitation band of the center emitting at 450 nm (Fig. 6a and b). Therefore, the conditions necessary for the energy transfer towards the center emitting at 450 nm are fulfilled, which is also another similarity with the observations reported for the Ce-doped $La_{0.86}Al_{11.9}O_{19.14}$ magnetoplumbite.[53]

Considering all these findings, it is very likely that the inclusions dominantly contain some Al-rich magnetoplumbite phases similar to those discussed above, or their mixtures, and they determine their luminescence behavior. The analysis of the composition of the inclusion in Fig. 4 shows a high content of Ce with respect to La. If the considerations on the composition of the inclusions are correct, the high Ce content would lead to decreased intensity of the short wavelength $Ce^{3+}$ emission and increased intensity of the long-wavelength emission related to the Ce–O associates. This is indeed observed in the cathodoluminescence spectrum in Fig. 5. The analysis in Fig. 4 shows some excess of the La(Ce) cations, which would be a sign of the presence of some other phase with a lower amount of Al with respect to La(Ce). It was not possible to confirm its composition by any of our methods.

Photoluminescence decay kinetics of the above peaks found in the spectra of the 30-H2-BS sample was studied to obtain better insight into the observed luminescence processes. The decay time of the emission of the regular $Ce^{3+}$ at the La site was found to be about 26 ns, while that of the Ce–O associates was about 40 ns. This is the consequence of the proportionality of the 5d–4f emission decay time to the third power of the emission wavelength.[54] The initial parts of the decay curves were obscured by some fast processes probably related to $F^+$-based centers, see paragraph 4 of the ESI† for details.

The selected samples were also studied under synchrotron radiation. For the 1-H2 sample very similar peaks were observed around 370 and 416 nm, while the former disappeared for 20% Ce concentration. Another peak was found at much longer wavelengths around 480 nm and its origin remains unknown. It also seems that an energy transfer from the LaAP matrix towards the inclusions under high energy excitation cannot take place. See paragraph 5 in the ESI† for details.

### 3.3. Luminescence properties of the selected Al-rich and LaAP powders

To further verify and better understand the luminescence processes in the grown crystals, the compounds prepared with the $LaAl_{11}O_{18}$ hexaaluminate (LHA) and the $La_{0.86}Al_{11.9}O_{19.14}$ magnetoplumbite (MP) stoichiometries with different Ce concentrations were studied together with the LaAP powders. All the Ce concentrations will be further denoted in atomic percents.

The radioluminescence spectra of the samples prepared by the solid state reaction with the $LaAl_{11}O_{18}$ stoichiometry with different Ce concentrations are shown in Fig. 7. The spectrum of the Ce-free sample peaks around 350 nm. With the increasing Ce concentration, it is slightly modified and shifts a bit towards longer wavelengths. For the Ce 1% sample a shoulder around 440 nm emerges, while it further shifts to longer wavelengths and becomes dominant for 20% Ce. This behavior

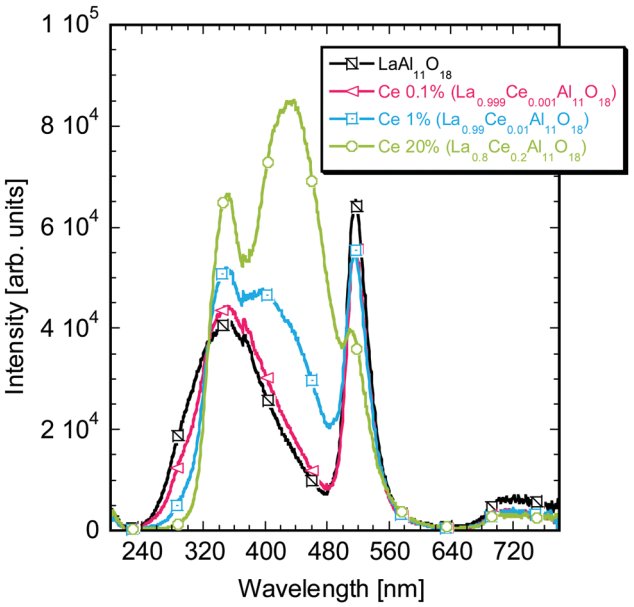


Fig. 7 Radioluminescence spectra of the $LaAl_{11}O_{18}$ samples with different Ce concentrations prepared *via* the solid state reaction.

is similar to that observed above for the inclusions and also for the MP compounds.[53] The short wavelength peaks somehow differ from those observed in the spectra for the inclusions (Fig. 3a and 6a), which might be caused by somewhat different compositions of the inclusions. They may consist of more aluminum rich phases.[52] An intense sharp band at 510 nm appears in all the powder samples and is tentatively ascribed to some defect related to the Al-rich matrix. It was not observed in the luminescence of the inclusions in the LaAP crystals, which again points to the fact that their composition may be different. The photoluminescence decay kinetics of the short wavelength peak in the UV region and the longer wavelength peak in the blue region roughly corresponded to those observed for the LaAP samples, see paragraphs 4 and 6 in the ESI.† The decay time of the former was about 20 ns while that of the latter around 40 ns. Energy transfer between the emission centers was confirmed in the powders, which is in accordance with the observations reported by Stevels.[53] As the photoluminescence decay kinetics of the PL peaks detected in the LaAP single crystal samples is obscured by some fast processes of unknown origin, the energy transfer could not be confirmed (see paragraph 4 in the ESI†).

The RL spectra of the samples based on the $La_{0.86}Al_{11.9}O_{19.14}$ MP powders prepared by the sol–gel method are shown in Fig. 8. The spectra somehow resemble those in Fig. 7 above, which supports the statement that $LaAl_{11}O_{18}$ LHA has a tendency to change its stoichiometry creating MP compounds.[52] The undoped sample shows a broad band centered around 370 nm extending towards longer wavelengths and the sharp 510 nm emission as well. Ce doping at low concentrations is responsible for the appearance of the 350 nm band. The intensity of this band reaches maximum for 1% Ce doping ($La_{0.8514}Ce_{0.0086}Al_{11.9}O_{19.14}$) and further decreases with increasing the Ce concentration in

favor of the long wavelength band around 440–450 nm. The 510 nm defect band is also observed, but it disappears for the highest Ce concentrations. The photoluminescence decay kinetics was quite similar to that of the LHA powders discussed above. It is necessary to mention that the undoped and low Ce-doped MP powders also show an intense emission in the blue region, which is most probably observed under UV-lamp excitation for some of the samples with low Ce concentration.

The data on the $LaAl_{11}O_{18}$- and $La_{0.86}Al_{11.9}O_{19.14}$-based samples are here treated just briefly in a way to draw a conclusion regarding the emission characteristics of the inclusions in the LaAP crystals. Further detailed treatment of the available results on these compounds would need separate intense research. We conclude that the phase responsible for the luminescence of the inclusions is some kind of Al-rich La magnetoplumbite with a composition close to that of $La_{0.86}Al_{11.9}O_{19.14}$. Other magnetoplumbite phases such as $La_{0.83}Al_{11.83}O_{19}$ or $LaAl_{11.67}O_{19}$ might play a role as well.[52]

The radioluminescence spectra of the Ce-doped LaAP powders contained mostly the luminescence of the $Cr^{3+}$ impurity around the 720 nm (see paragraph 7 in ESI†). A flat unstructured weak emission was observed at shorter wavelengths and no ascription was possible. For the low Ce concentration, a broad band was observed around 600 nm and it might be again related to some $Ce^{3+}$–$Cr^{3+}$ interactions as was discussed above.

### 3.4. Electron paramagnetic resonance studies

The measurements of the undoped sample at low temperatures have revealed the $Cr^{3+}$, $Fe_{3+}$ and $Ir^{4+}$ impurities together with the $O^-$ center, see paragraph 8 of the ESI.†

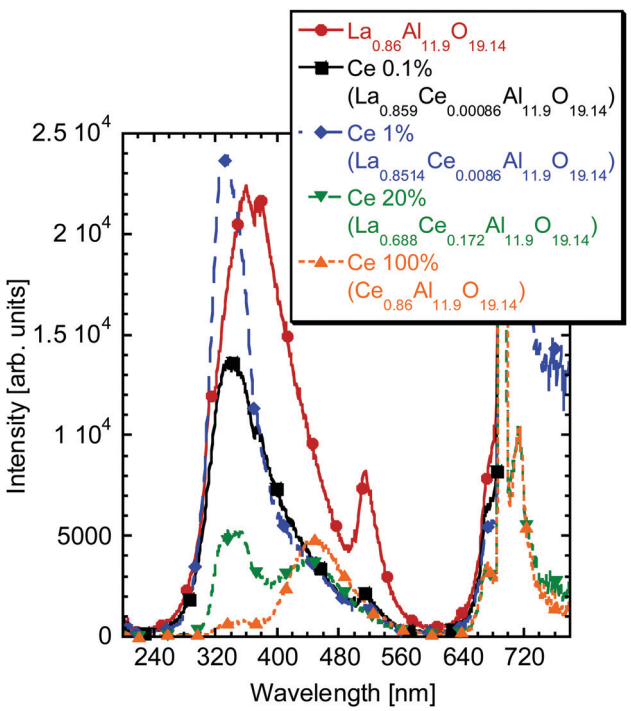


Fig. 8 Radioluminescence spectra of the $La_{0.86}Al_{11.9}O_{19.14}$-based samples with different Ce concentrations prepared by the sol–gel process.

The EPR spectra of the Ce-doped LaAP 1-N2, 1-H2, 20-N2 and 20-H2 recorded at 5 K are compared in Fig. 9 with those of the 0.5-N2, 50-N2 and 50-H2 samples. One can immediately see that the spectra differ drastically upon the cerium content. A lower doping level (1%) results in several more or less narrow components whereas 20% ends up with the very broad ones as expected. Strikingly, the component positions in the 1% and 20% are not the same. At least four distinct groups of lines can be distinguished in both samples and are found at the $g$ factors: $g_1 = 2.38$, $g_2 = 1.92$, $g_3 = 0.96$ (Ce1); $g_1 = 3.04$, $g_2 = 1.39$, $g_3 = 1.06$ (Ce2); $g = 2.11$ (Nd); and $g_1 \sim 3.81$, $g_3 = 0.88$ (Ce3). The Ce1 signal, clearly resolved, seems to exist only in LaAP:Ce1% for both growth atmospheres. The $g_3 = 1.06$ broad resonance line (at approximately 6300 G) may also be strengthened by magnetic ordering that occurred due to a large amount of the neighboring $Ce^{3+}$ ions.[55] The Nd signal can be clearly observed only in the LaAP:0.5%Ce and both LaAP:1%Ce samples. The corresponding resonances were ascribed to $Nd^{3+}$ considering the temperature dependence of the signals – they are not

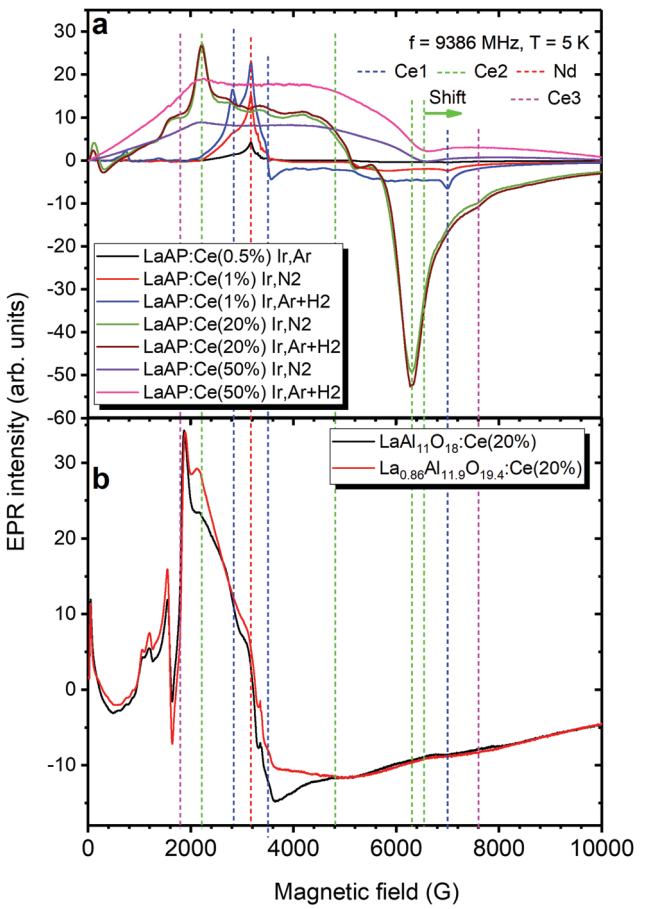


Fig. 9 (a) EPR spectra recorded for the LaAP:Ce samples indicated in a legend. Resonance lines originating from different cerium ions (Ce1-3) and neodymium ions (Nd) are stressed by dashed vertical lines distinguished by colour. "Shift" indicates the shift of the g factor position in the LaAP:Ce50% as compared to the LaAP:Ce20% sample. (b) EPR spectra recorded for the 20% Ce doped $LaAl_{11}O_{18}$ hexaaluminate and $La_{0.86}Al_{11.9}O_{19.14}$ magnetoplumbite as indicated in the legend.

observed at about 20–30 K but appear only at 5–9 K. This is not typical for $Ce^{3+}$ ions but fully in line with $Nd^{3+}$.[40,41,56] Moreover, the corresponding $g$ factors are typical for $Nd^{3+}$. The Ce2,3 signals are dominating in LaAP:Ce20%. Based on the temperature dependence of the Ce1-3 signals and the observed correlation between the EPR signal intensities and the cerium content in the samples, the Ce1-3 signals were ascribed to $Ce^{3+}$ ions located at different surroundings.

The $g_1$ = 3.04 of the Ce2 seems to be close to the $g_z$ = 3.565 value of the **g** tensor reported for instance for YAP ($g_z$ = 3.565, $g_y$ = 0.395, and $g_x$ = 0.21).[40] The other two values, $g_{2,3}$, differ more than twice from $g_{x,y}$. The positions of the typical $g$ factor values of the Ce2 could be found to be almost the same in LaAP:Ce50% as well: $g_1$ = 3.04, $g_3$ = 1.03 (Fig. 9a). The $g_2$ value could not be determined precisely in LaAP:Ce50% because of the very strong broadening. This allows us to assume that Ce2 appears as $Ce^{3+}$ in the CeAP phase created in the LaAP matrix as another structure. The small shift of the $g_3$ value from 1.06 in LaAP:Ce20% to 1.03 in LaAP:Ce50% can be explained by the different sizes of the CeAP inclusions and resulting different tensions acting on the CeAP particles in LaAP:Ce20% and LaAP:Ce50%, respectively.

On the other hand, the Ce1 $g$ factors differ very much from the **g** tensor values reported for YAP ($g_1$ = 3.565, $g_2$ = 0.395, and $g_3$ = 0.21)[40] and also differ much from those of Ce2. The structure of LaAP is $R\bar{3}c$ below 430 °C supposing axial symmetry of the La site so that $Ce^{3+}$ replacing La should yield axial **g** tensor values, *e.g.*, $g_1 = g_2 = g_\perp$ and $g_3 = g_\parallel$. The $g_1$ = 2.38 and $g_2$ = 1.92 of Ce1, however, are not enough spectrally separated, and therefore, based on these considerations, the Ce1 center is expected to be the $Ce^{3+}$ embedded at La site but somehow perturbed, probably, the off-center ion in the LaAP.

Since the hexaaluminate $LaAl_{11}O_{18}$ and magnetoplumbite $La_{0.86}Al_{11.9}O_{19.14}$ phases are supposed to be present in the LaAP samples studied, to find out whether $Ce^{3+}$ appears in these phases the cerium doped $LaAl_{11}O_{18}$ and $La_{0.86}Al_{11.9}O_{19.14}$ materials were examined by EPR spectroscopy as well. In particular, the EPR spectra of $Ce^{3+}$ in these materials are shown in the Fig. 9b for the 20% doping level. The $Ce^{3+}$ resonances were distinguished on the basis of the correlation observed between the level of Ce doping and the EPR intensity. The Ce3 resonances in Fig. 9a, can now be compared with the $Ce^{3+}$ resonances observed in the $LaAl_{11}O_{18}$ and $La_{0.86}Al_{11.9}O_{19.14}$ materials (see Fig. 9b). The positions of the Ce3 resonance lines are in good agreement with the $Ce^{3+}$ resonances in the $LaAl_{11}O_{18}$:Ce20% and $La_{0.86}Al_{11.9}O_{19.14}$:Ce20% materials. This allows assuming that indeed at least some part of $Ce^{3+}$ appears within the hexaaluminate or magnetoplumbite-like inclusions at higher cerium doping levels in the LaAP crystals. This is in good agreement with the luminescence measurements above.

The growth atmosphere had a relatively strong effect on the overall spectral intensity as shown in Fig. 9a. Reducing conditions seem prosperous for $Ce^{3+}$ incorporation especially for the 1% concentration where the EPR signal was increased 1.5 times compared to that under the neutral atmosphere. Note, that during samples synthesis, Ce in the precursor is in the 4+ charge state. Hydrogen, naturally reduces it to 3+. This is the reason for the $Ce^{3+}$ EPR signal improvement in the samples grown under a reducing atmosphere. In particular, the Ce1 signal becomes strongly dominating in LaAP, proving that the Nd signals indeed belong to $Nd^{3+}$ which cannot be reduced by hydrogen.

## 4. Luminescence mechanism in the LaAP:Ce single crystals

Since a blue luminescence similar to that one coming from the inclusions in our samples was observed by Zeng *et al.* in the Czochralski-grown crystals,[15] we can infer that such Al-rich inclusions were created in those crystals as well. This again supports the assumption that inclusions are created in LaAP crystals grown from the melt and this can happen regardless of the growth method. The schematic of the luminescence mechanism is sketched in Fig. 10. The broad band observed

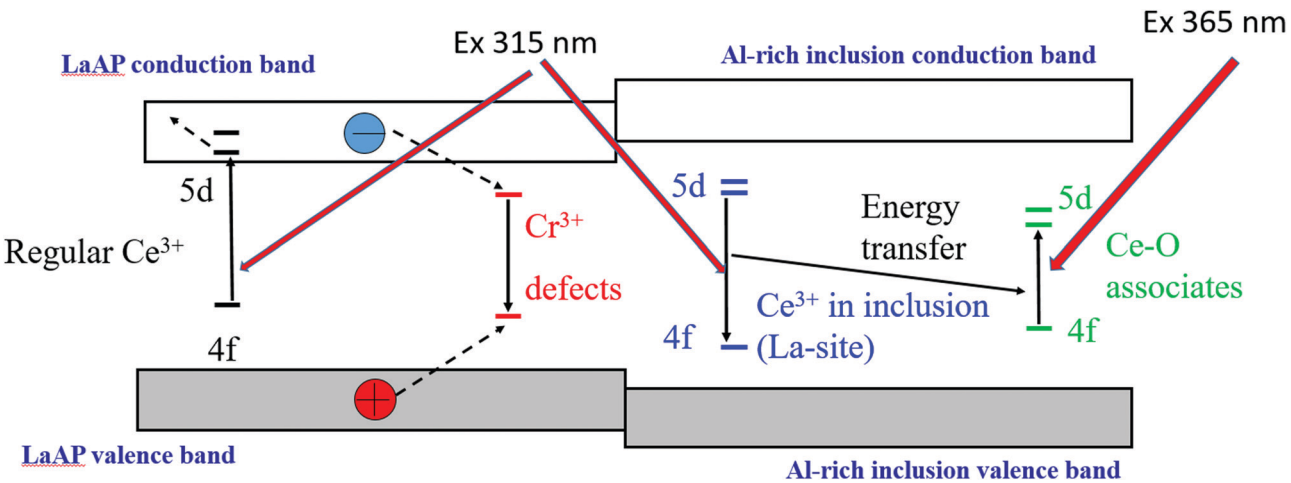


Fig. 10 Schematic of the possible luminescence mechanism in LaAP:Ce crystals. The level positions are just schematic and do not reflect their mutual positions or positions with respect to the valence and conduction bands.

by Zeng *et al.*[35] was peaking at 410 nm and was excited at 317 nm. The 410 nm peak would correspond to the emission of the Ce–O associates in the Al-rich magnetoplumbite inclusions, whose 5d excited levels are populated *via* energy transfer from the excited 5d levels of the regular $Ce^{3+}$ residing at the La site in the inclusion. The $Ce^{3+}$ residing in the regular La site is excited with the 317 nm light. This excitation wavelength corresponds well with the $Ce^{3+}$ 4f–5d absorption in the LaAP matrix, which gives an impression that the emission around 410 nm originates from $Ce^{3+}$ in LaAP, which was concluded by Zeng *et al.*[35] The reported 317 nm excitation and 410 nm emission wavelengths are slightly different from those observed by us, but no spectral corrections have been reported[35] and therefore these values might come from the uncorrected spectra.

From the above results we consider that $Ce^{3+}$ incorporated in LaAP is not luminescent, since its 5d states are buried in the conduction band and the luminescence quenching by the 5d excited state ionization takes place, as was observed by van der Kolk *et al.*[37] Since the $Ce^{3+}$ levels were studied by photoconductivity,[37] such an experiment simply could not detect the isolated inclusions in the material, even if they were present. The $Cr^{3+}$ impurity in the LaAP matrix is responsible for the red emission and can also take part in the cooperative Ce-terminated luminescence in the orange-red regions. The $Cr^{3+}$ impurity levels can be populated under excitation with ionizing radiation and take part in the described processes. Some unknown defects can also play a role in the luminescence processes, especially in the undoped samples. It seems that the excitation energy released in the material by ionizing radiation cannot be efficiently transferred towards the inclusions, unless their concentration is high enough, as was observed for the seed part of the 30-H2-BS sample, see Fig. 2. There is a question of what is the band-gap of the compounds constituting the inclusions. It is reasonable to assume it is larger than that for LaAP, if one considers the band gap value of 5.6 eV for LaAP[34] and 7 or 7.6 eV for $Al_2O_3$ depending on its modification.[57] In that case the charge carriers generated by the ionizing radiation and migrating in the LaAP matrix simply cannot transfer energy to the inclusions and their luminescence could be excited only by the UV light, which is indeed observed. Thus, the LaAP:Ce single crystals do not give any scintillation response, but can show blue photoluminescence under UV excitation due to Al-rich inclusions created during growth. Therefore, we believe that van der Kolk *et al.* studied the quenching of regular $Ce^{3+}$ in the LaAP matrix,[37] while Zeng *et al.*[35] observed Al-rich inclusion luminescence, which could be excited by a wavelength very similar to the $Ce^{3+}$ 4f–5d absorption in LaAP and such an observation might have led to confusion. Practically, there is no controversy in the literature and it simply seems that both teams observed different phenomena which can coexist simultaneously in this material. We note that the valence and conduction bands of the inclusion in Fig. 10 are drawn just tentatively and their position cannot be reliably determined from the presented results. It is necessary to note that the luminescence of the Ce–O associates can be excited directly by wavelengths around 365 nm (Fig. 10). Therefore, the LaAP:Ce crystals containing the Al-rich inclusions can exhibit blue luminescence under a mercury UV lamp (medium pressure) excitation.

## 5. Inclusion creation and reasons for nonstoichiometry of LaAP

It is necessary to explain why we can observe the Al-rich inclusion luminescence in the samples with the balanced stoichiometry. The answer might be found in Fig. S2 in the ESI† (paragraph 1). It shows the DSC-TGA-MS analyses of the $La_2O_3$ starting powder pre-heated under the $N_2$ atmosphere up to 1200 °C and kept in a glovebox under the $N_2$ protective atmosphere ($H_2O < 1$ ppm, $O_2 < 1$ ppm) for 5 days. The peaks of $H_2O$ and $CO_2$ escape are visible, though with the intensities 1–2 orders of magnitude smaller than those for the untreated powder from the supplier, see Fig. S1 and S2 in the ESI.† The total mass of the escaped substances is about 0.25% in total, which may already have led to a non-negligible weighing error. Further research is needed to find where the absorbed substances come from. Maybe the pre-heating process was somehow insufficient or there might be a problem of adsorption of the substances on the polyethylene container where the starting powder is stored in the glovebox. The former can be most probably excluded since the DSC-TGA measurements of the freshly heated powder did not show any effects related to the release of $H_2O$ or $CO_2$.

We have also performed the mass increase rate test for the freshly baked $La_2O_3$ powder (0.5 g) which was exposed to air under laboratory conditions, see Fig. S3 in the ESI† (paragraph 1). In about 1 hour, the mass increased by 1 wt%, which is a bit surprising result. In 5 days, the mass increase was saturated at the value of about 15 wt%. Weighing of a $La_2O_3$ starting material for the crystal growth was performed either in a glovebox or very quickly (in few minutes) in air. Thus, this source of error can be excluded; however, one must be aware of such behavior of $La_2O_3$. It is necessary to emphasize that in the first 100 minutes $La_2O_3$ can be surprisingly as hygroscopic as $LaCl_3$ or $EuBr_2$; see paragraph 1 (Fig. S3) in the ESI† and observations in other reports.[58] It is important to bear this also in mind when preparing other La-containing multicomponent oxides.

## 6. Conclusions

The combined investigation of the absorption, luminescence and electron paramagnetic resonance spectroscopies of the Ce-doped LaAP single crystals, further supported by the SEM analysis, has explained the origin of blue luminescence sometimes observed in this material. It was ascribed to the $Ce^{3+}$ emission in the aluminum-rich inclusions often created in the material due to its non-stoichiometry caused most probably by weighing errors in the crystal growth procedure. They are related to the $La_2O_3$ starting material's hygroscopicity and ability to absorb $CO_2$ from air or even from the protective

atmosphere with high purity. The composition of the inclusions corresponds to some lanthanum aluminate with a magnetoplumbite structure, such as $La_{0.86}Al_{11.9}O_{19.14}$ or similar. The $Ce^{3+}$ resides in such a compound either at the regular La-site giving rise to the UV emission around 370 nm or at the distorted La-site, which results in blue emission around 440 nm. Energy transfer from the former emission center towards the latter one most probably takes place. Due to the energy transfer the blue 440 nm emission can be excited also by the wavelength which is very close to the 4f–5d absorption of $Ce^{3+}$ in the LaAP matrix. Such a phenomenon was most probably misinterpreted by some researchers who erroneously ascribed the blue emission to the $Ce^{3+}$ luminescence in the LaAP matrix. The $Ce^{3+}$ in LaAP is not luminescent due to the engulfment of its 5d states by the conduction band. Even though the luminescence of the inclusions can be efficient in the photoluminescence processes, due to the isolation of the inclusions in the matrix and their different electronic structures, their luminescence cannot take part in the scintillation process during excitation by ionizing radiation. Therefore, possible usage of the Ce-doped LaAP as a scintillation material can be finally definitely excluded.

## Author contributions

J. Pejchal: conceptualization, methodology, project administration, resources, supervision, writing – original draft, and writing – review and editing. V. Babin: investigation, visualization, and formal analysis. M. Buryi: investigation, visualization, methodology, writing – original draft, and writing – review and editing. V. Laguta: investigation, visualization, and resources. F. Hájek: investigation, visualization, and resources. J. Páterek: investigation, visualization, resources, and formal analysis. L. Procházková-Prouzová: investigation, and writing – review and editing. L. Havlák: Investigation, resources, methodology, validation, and writing – original draft. V. Czerneková: investigation and validation. V. Vaněček: investigation, visualization, and validation. V. Doležal: investigation. J. Havlíček: investigation. K. Rubešová: investigation, resources, validation, supervision, and writing – original draft. P. Zemenová: investigation and visualization. A. Falvey: investigation. R. Král: investigation, methodology, and writing – original draft. V. Pankratov: project administration and resources. K. Chernenko: investigation and resources.

## Conflicts of interest

There are no conflicts to declare.

## Acknowledgements

The work was supported by the Czech Science Foundation project no. 18-14789S and by Operational Programme Research, Development and Education financed by European Structural and Investment Funds and the Czech Ministry of Education, Youth and Sports (Project No. SOLID21 CZ.02.1.01/0.0/0.0/16_019/0000760). We acknowledge MAX IV Laboratory for time on Beamline FinEstBeAMS under Proposal 20180572. The research leading to this result was supported by the project CALIPSOplus under the Grant Agreement 730872 from the EU Framework Programme for Research and Innovation HORIZON 2020. The Institute of Solid State Physics, University of Latvia as the Center of Excellence has received funding from the H2020-WIDESPREAD-01-2016-2017-Teaming Phase2 under Grant Agreement No. 739508, Project CAMART2.

## References

1 M. Nikl and A. Yoshikawa, *Adv. Opt. Mater.*, 2015, **3**, 463.
2 P. A. Rodnyi, *Physical processes in inorganic scintillators*, CRC Press, Boca Raton, 1997.
3 D. Creagh, *Radiat. Phys. Chem.*, 2014, **95**, 50.
4 P. Lecoq, *Nucl. Instrum. Methods Phys. Res., Sect. A*, 2016, **809**, 130.
5 Y. Shikaze, Y. Nishizawa, Y. Sanada, T. Torii, J. Jiang, K. Shimazoe, H. Takahashi, M. Yoshino, S. Ito, T. Endo, K. Tsutsumi, S. Kato, H. Sato, Y. Usuki, S. Kurosawa, K. Kamada and A. Yoshikawa, *J. Nucl. Sci. Technol.*, 2016, **53**, 1907.
6 Science Alert, https://www.sciencealert.com/drone-flyovers-of-chernobyl-reveal-incredible-radiation-hotspots-in-unprecedented-detail (accessed March 2021).
7 M. Nikl, A. Yoshikawa, K. Kamada, K. Nejezchleb, C. R. Stanek, J. A. Mares and K. Blazek, *Prog. Cryst. Growth Charact. Mater.*, 2013, **59**, 47.
8 Y. Evangelista, F. Fiore and F. Fuschino, *et al.*, in *Space Telescopes and Instrumentation 2020: Ultraviolet to Gamma Ray*, ed. J.-W. A. den Herder, K. Nakazawa and S. Nikzad, SPIE, United States, Online Only, 2020, p. 168, DOI: 10.1117/12.2561018.
9 M. Nikl, V. V. Laguta and A. Vedda, *Phys. Status Solidi B*, 2008, **245**, 1701.
10 L. Pidol, B. Viana, A. Bessière, A. Galtayries, P. Dorenbos and B. Ferrand, *Mater. Sci. Forum*, 2007, **555**, 371.
11 A. Yoshikawa, S. Kurosawa, Y. Shoji, V. I. Chani, K. Kamada, Y. Yokota and Y. Ohashi, *Cryst. Growth Des.*, 2015, **15**, 1642.
12 J. Iwanowska-Hanke, M. Moszynski, P. Sibczynski, K. Brylew, A. Dziedzic, A. Yoshikawa and K. Kamada, in 2017 IEEE NSS/MIC, IEEE, Atlanta, GA, 2017, pp. 1–3.
13 R. Král, P. Zemenová, V. Vaněček, A. Bystřický, M. Kohoutková, V. Jarý, S. Kodama, S. Kurosawa, Y. Yokota, A. Yoshikawa and M. Nikl, *J. Therm. Anal. Calorim.*, 2020, **141**, 1101.
14 R. Kral, V. Jary, J. Pejchal, S. Kurosawa, K. Nitsch, Y. Yokota, M. Nikl and A. Yoshikawa, *IEEE Trans. Nucl. Sci.*, 2016, **63**, 453.
15 D. J. Singh, *Phys. Rev. B: Condens. Matter Mater. Phys.*, 2010, **82**, 155145.
16 E. D. Bourret-Courchesne, G. A. Bizarri, R. Borade, G. Gundiah, E. C. Samulon, Z. Yan and S. E. Derenzo, *J. Cryst. Growth*, 2012, **352**, 78.

17 L. Stand, M. Zhuravleva, B. Chakoumakos, H. Wei, J. Johnson, V. Martin, M. Loyd, D. Rutstrom, W. McAlexander, Y. Wu, M. Koschan and C. L. Melcher, *J. Lumin.*, 2019, **207**, 70.
18 P. Lecoq, I. Dafinei, E. Auffray, M. Schneegans, M. V. Korzhik, O. V. Missevitch, V. B. Pavlenko, A. A. Fedorov, A. N. Annenkov, V. L. Kostylev and V. D. Ligun, *Nucl. Instrum. Methods Phys. Res., Sect. A*, 1995, **365**, 291.
19 M. J. Weber and R. R. Monchamp, *J. Appl. Phys.*, 1973, **44**, 5495.
20 M. J. Weber, *J. Appl. Phys.*, 1973, **44**, 3205.
21 E. Gumanskaya, A. O. Egorycheva, M. V. Korzhik, S. A. Smirnova, V. B. Pavlenko and A. A. Fedorov, *Opt. Spectrosc.*, 1992, **72**, 395.
22 A. G. Petrosyan, G. O. Shirinyan, C. Pedrini, C. Durjardin, K. L. Ovanesyan, R. G. Manucharyan, T. I. Butaeva and M. V. Derzyan, *Cryst. Res. Technol.*, 1998, **33**, 241.
23 C. Dujardin, C. Pedrini, W. Blanc, J. C. Gâcon, J. C. van't Spijker, O. W. V. Frijns, C. W. E. van Eijk, P. Dorenbos, R. Chen, A. Fremout, F. Tallouf, S. Tavernier, P. Bruyndonckx and A. G. Petrosyan, *J. Phys.: Condens. Matter*, 1998, **10**, 3061.
24 A. Lempicki and R. H. Bartram, *J. Lumin.*, 1999, **81**, 13.
25 M. Nikl, *Phys. Status Solidi A*, 2000, **178**, 595.
26 J. Trummer, E. Auffray, P. Lecoq, A. Petrosyan and P. Sempere-Roldan, *Nucl. Instrum. Methods Phys. Res., Sect. A*, 2005, **551**, 339.
27 V. V. Laguta, M. Nikl, A. Vedda, E. Mihokova, J. Rosa and K. Blazek, *Phys. Rev. B: Condens. Matter Mater. Phys.*, 2009, **80**, 045114.
28 P. Dorenbos, *IEEE Trans. Nucl. Sci.*, 2010, **57**, 1162.
29 R. S. Roth, *J. Res. NBS*, 1957, **58**, RP2736.
30 S. J. Schneider and R. S. Roth, *J. Res. Natl. Bur. Stand., Sect. A*, 1960, **64A**, 317.
31 S. Geller and V. B. Bala, *Acta Crystallogr.*, 1956, **9**, 1019.
32 M. Faucher and P. Caro, *J. Chem. Phys.*, 1975, **63**, 446.
33 J. Pejchal, J. Barta, T. Trojek, R. Kucerkova, A. Beitlerova and M. Nikl, *Radiat. Meas.*, 2019, **121**, 26.
34 P. W. Peacock and J. Robertson, *J. Appl. Phys.*, 2002, **92**, 4712.
35 X. Zeng, L. Zhang, G. Zhao, J. Xu, Y. Hang, H. Pang, M. Jie, C. Yan and X. He, *J. Cryst. Growth*, 2004, **271**, 319.
36 G. Blasse and A. Bril, *J. Chem. Phys.*, 1967, **47**, 5139.
37 E. van der Kolk, J. T. M. de Haas, A. J. J. Bos, C. W. E. van Eijk and P. Dorenbos, *J. Appl. Phys.*, 2007, **101**, 083703.
38 E. Auffray, S. Baccaro, T. Beckers and Y. Benhammou, *et al.*, *Nucl. Instrum. Methods Phys. Res., Sect. A*, 1996, **383**, 367.
39 P. Arhipov, S. Tkachenko, I. Gerasymov, O. Sidletskiy, K. Hubenko, S. Vasyukov, N. Shiran, V. Baumer, P. Mateychenko, A. Fedorchenko, Y. Zorenko, Y. Zhydachevskii, K. Lebbou and M. Korjik, *J. Cryst. Growth*, 2015, **430**, 116.
40 M. Buryi, V. V. Laguta, E. Mihóková, P. Novák and M. Nikl, *Phys. Rev. B: Condens. Matter Mater. Phys.*, 2015, **92**, 224105.
41 M. Buryi, V. Laguta, M. Nikl, V. Gorbenko, T. Zorenko and Y. Zorenko, *CrystEngComm*, 2019, **21**, 3313.
42 A. Yoshikawa and V. Chani, *MRS Bull.*, 2009, **34**, 266.
43 A. Yoshikawa, M. Nikl, G. Boulon and T. Fukuda, *Opt. Mater.*, 2007, **30**, 6.
44 E. Mihóková, M. Nikl, M. Bacci, M. Dušek and V. Petříček, *Phys. Rev. B: Condens. Matter Mater. Phys.*, 2009, **79**, 195130.
45 Z. Song and Q. Liu, *Phys. Chem. Chem. Phys.*, 2019, **21**, 2372.
46 H. Luo and P. Dorenbos, *J. Mater. Chem. C*, 2018, **6**, 4977.
47 P. Dorenbos, *Phys. Rev. B: Condens. Matter Mater. Phys.*, 2012, **85**, 165107.
48 P. Dorenbos, *J. Lumin.*, 2002, **99**, 283.
49 P. Wu and A. D. Pelton, *J. Alloys Compd.*, 1992, **179**, 259.
50 V. Singh, G. Sivaramaiah, J. L. Rao, R. Senthil Kumaran and S. J. Dhoble, *J. Nanosci. Nanotechnol.*, 2016, **16**, 789.
51 V. Singh, N. Singh, M. S. Pathak, S. Watanabe, T. K. Gundu Rao, P. K. Singh and V. Dubey, *Optik*, 2018, **157**, 1391.
52 J.-G. Park and A. N. Cormack, *J. Eur. Ceram. Soc.*, 1999, **19**, 2249.
53 A. L. N. Stevels, *J. Electrochem. Soc.*, 1978, **125**, 588.
54 P. Dorenbos, M. Marsman, C. W. E. Van Eijk, M. V. Korzhik and B. I. Minkov, *Radiat. Eff. Defects Solids*, 1995, **135**, 325.
55 R. Díaz-Pardo and R. Valenzuela, in *Advanced Electromagnetic Waves*, ed. S. Bashir, InTech, 2015.
56 M. Buryi, V. Laguta, V. Babin, O. Laguta, M. G. Brik and M. Nikl, *Opt. Mater.*, 2020, **106**, 109930.
57 E. O. Filatova and A. S. Konashuk, *J. Phys. Chem. C*, 2015, **119**, 20755.
58 M. Zhuravleva, L. Stand, H. Wei, C. Hobbs, L. Boatner, K. Shah, A. Burger, P. Bhattacharya, E. Tupitsyn and C. Melcher, In 2013 IEEE NSS/MIC, IEEE, Seoul, Korea (South), 2013, pp. 1–5.